ELECTRONIC SUPPLEMENTARY INFORMATION

An artificial photosynthetic system for photoaccumulation of two electrons on a fused dipyridophenazine (dppz) – pyridoquinolinone ligand

Jean-François Lefebvre,[a,b] Julian Schindler,[c,d] Philipp Traber,[c] Ying Zhang,[c,d] Stephan Kupfer,[c] Stefanie Gräfe,[c] Isabelle Baussanne,[b] Martine Demeunynck,[b] Jean-Marie Mouesca,[f] Serge Gambarelli,[f] Vincent Artero,[a] Benjamin Dietzek,[*c,d,e] Murielle Chavarot-Kerlidou[*a]

Email: murielle.chavarot-kerlidou@cea.fr; benjamin.dietzek@leibniz-ipht.de

[a] Laboratoire de Chimie et Biologie des Métaux, Univ. Grenoble Alpes, CNRS, CEA, 38000 Grenoble, France.

[b] Univ. Grenoble Alpes, CNRS, DPM, 38000 Grenoble, France.

[c] Institute of Physical Chemistry and Abbe Center of Photonics, Friedrich Schiller University Jena, Helmholtzweg 4, 07743 Jena, Germany.

[d] Department Functional Interfaces, Leibniz Institute of Photonic Technology Jena (IPHT), Albert-Einstein-Straße 9, 07745 Jena, Germany.

[e] Center for Energy and Environmental Chemistry, Friedrich Schiller University Jena, Philosophenweg 8, 07743 Jena, Germany.

[f] Univ. Grenoble Alpes, CEA, CNRS, INAC-SyMMES, 38000 Grenoble, France.

General.

^{1}H NMR and ^{13}C NMR spectra were recorded at 298 K in 5 mm o.d. tubes either on a *Bruker AC 300* spectrometer equipped with a QNP probe head operating at 300.0 MHz for ^{1}H and 75.5 MHz for ^{13}C or on a *Bruker Avance III* spectrometer equipped with a *Prodigy* cryoprobe and operating at 500.0 MHz for ^{1}H and 126 MHz for ^{13}C. UV-vis absorption spectra were recorded on an Agilent Technologies Cary 60 UV-Vis spectrometer, equipped with optical fibers and an external cell holder for measurements inside the glovebox. Chemical shift values are given in ppm with reference to solvent residual signals. Accurate mass measurements (HRMS) were performed on a Bruker maXis mass spectrometer by the "Fédération de Recherche" ICOA/CBM (FR 2708) platform and elemental analysis on a Thermofisher Scientific "Flash 2000" by the "Plateforme d'analyse pour la chimie" (GDS 3648, Strasbourg).

Synthesis.

All reagents were obtained from commercially available sources and used without further purification. Solvents were dried from appropriate drying agents and freshly distilled under argon before use. Chemical reagents were purchased from Sigma-Aldrich and used as received. Complex $[Ru(bpy)_2(dppz)](PF_6)_2$ was prepared according to reported procedure.

$[Ru(bpy)_2(oxo\text{-}dppqp)](PF_6)_2$ ($[1](PF_6)_2$). $[Ru(bpy)_2(dppqp)](PF_6)_2$ (0.1 g, 8.6 x10^{-5} mol) was dissolved in acetonitrile (15 mL) in the dark. Ceric ammonium nitrate (0.172 g, 3.14x10^{-4} mol, 3.65 eq.) dissolved in water (7 mL) was added and the mixture was stirred for 2 hours at room temperature in the dark. Aqueous ammonium hexafluorophosphate (10 mL) was then added to precipitate the product. The solid was filtered, washed with water and dried. The crude was purified by column chromatography on silica gel using a gradient of aqueous 10% KNO_3 solution in acetonitrile as eluent. The product was precipitated by adding NH_4PF_6 in the aqueous residue, filtered, washed with water and dried. The solid was solubilised in a small amount of acetonitrile and precipitated with diethylether. Filtration, washings with diethyl ether and drying afforded 78 mg of pure **$[1](PF_6)_2$** as a red solid in 80% yield.

^{1}H NMR (CD_3CN, 25°C, 500 MHz, 5x10^{-3} mol.L^{-1}): δ 9.80 (d, *J* = 8.0 Hz, 1H), 9.66 (d, *J* = 7.9 Hz, 1H), 9.50 (d, *J* = 9.3 Hz, 1H), 9.49 (d, *J* = 4.4 Hz, 1H), 8.62 - 8.54 (m, 4H), 8.54 (d, *J* = 9.3 Hz, 1H), 8.27 (d, *J* = 5.2 Hz, 2H), 8.18 - 8.13 (m, 2H), 8.10 (d, *J* = 4.4 Hz, 1H), 8.08 (d, *J* = 10.1 Hz, 1H), 8.08 - 8.03 (m, 2H), 7.97 (dd, *J* = 8.0 and 5.2 Hz, 1H), 7.92 (dd, *J* = 7.9 and 5.2 Hz, 1H), 7.90 (d, *J* = 5.8 Hz, 2H), 7.86 (d, *J* = 5.5 Hz, 1H), 7.83 (d, *J* = 5.5 Hz, 1H), 7.53 - 7.48 (m, 2H), 7.35 - 7.29 (m, 2H), 6.94 (d, *J* = 10.1 Hz, 1H). **^{13}C NMR** (CD_3CN, 25°C, 75 MHz, 2.5x10^{-2} mol.L^{-1}): δ 185.3, 158.2, 158.1, 157.0, 155.2, 155.0, 153.3, 153.2, 153.0, 153.0, 152.1, 151.9, 151.5, 151.4, 147.4, 145.2, 144.6,

144.2, 141.7, 141.3, 140.6, 139.1, 139.0, 134.7, 134.7, 134.6, 134.6, 131.8, 131.3, 131.2, 128.7, 128.6, 128.5, 128.5, 127.1, 125.4, 125.4, 121.9, 117.9 ppm. **UV-visible** (CH_3CN): λ_{max} in nm (ε in $L.mol^{-1}.cm^{-1}$) 244 (49500), 257 (53700), 287 (101100), 315 (83100), 351 (20250), 367 (20280), 394 (sh 23750), 418 (31200). **HRMS (ESI$^+$)**: calcd for $C_{47}H_{28}N_{10}ORu$: 425,0746, found: 425.0749 ($[M]^{2+}$), calcd for $C_{47}H_{28}F_6N_{10}OPRu$: 995.1140, found: 995.1129 ($[M + PF_6]^+$). **E.A.**: calcd for $C_{47}H_{28}F_{12}N_{10}OP_2Ru \bullet 0{,}3NH_4PF_6$: N 12.10, C 47.56, H 2.54; found: N 11.93, C 47.59, H 2.65.

Electrochemical Measurements:

Electrochemical analysis was performed using a BioLogic SP300 potentiostat controlled via EC-Lab V10 software. Cyclic and differential pulse voltammetry experiments were recorded in a classical single-compartment three-electrode cell combining a glassy carbon or a platinum working electrode, a platinum wire counter electrode, and a custom-made Ag/AgCl reference electrode (separated from the solution by a Vycor frit). Typical measurements were carried out at room temperature using 3 mL of argon-purged solution of complex in DMF (0.1 M n-Bu_4NPF_6 as supporting electrolyte). Measurements were corrected for ohmic drop. Ferrocene was finally added at the end of each measurement as an internal reference, allowing every measured value to be referenced versus the Fc^+/Fc redox couple.

Procedure for the chemical reduction of $[1](PF_6)_2$:

All the experiments were realized in a glovebox. All volume measurements and dilution were done using micropipettes. Experiments were carried out in either 1 cm or 2 mm quartz cuvettes and monitored by UV-vis spectroscopy inside the glovebox.

Cobaltocene (Cp_2Co) stock solutions: The solution of Cp_2Co for each *UV-visible monitoring* was prepared in dry and degassed acetonitrile (approximately 1.5 mM). A 1 cm cuvette was filled with 3 mL of dry, degassed acetonitrile and aliquots of 30 µL were added. The concentration of Cp_2Co in the cuvette was determined by the increase in absorption between two successive additions of stock solution according to the molar absorptivity found in the literature[1] ($\varepsilon_{(327nm)}$ = 742 $m^2.mol^{-1}$ *ie* 7420 $L.mol^{-1}.cm^{-1}$ in ethanol). The accurate concentration of the stock solution was then calculated as well as the excess of Cp_2Co necessary to quench any residual oxygen in the 3 mL of acetonitrile (using the difference of absorption due to the first aliquot compared to the next ones). Our results were in agreement with the previous results reported by the group of Frederick MacDonnell, where 0,2 equivalents excess was used.

[1] A. Jaworska-Augustyniak, J. Wojtczak, *Monatshefte für Chemie*, **1979**, *110*, 1113-1121.

TFA stock solution: 10 mM and 1.5 mM stock solutions of TFA in dry, degassed acetonitrile were prepared by dilution. Both solutions were kept in the freezer.

UV-visible monitoring: UV-vis absorption spectra were recorded on a Cary 60 UV-vis (Agilent Technologies) spectrophotometer, equipped with optical fibers to record spectra in the glovebox. Different 1 cm cuvettes were filled with 3 mL of the same 15 µM solution of complex **[1](PF$_6$)$_2$** in dry and degassed acetonitrile (prepared from a 150 µM stock solution). Chemical reduction and protonation were carried out by adding aliquots of the 1.5 mM Cp_2Co or TFA solution in the cuvette with stirring before UV-vis spectrum measurement. The recovery of the solution was monitored by taking out the sample from the glovebox and exposing it to air before UV-vis spectrum measurements.

Procedure for the EPR spectroscopy:

A 2 mm cuvette was filled with 0.5 mL of a 200 µM solution of complex **[1](PF$_6$)$_2$** in acetonitrile/ propionitrile (1/2). The chemical reduction was carried out by adding aliquots of a Cp_2Co stock solution (10 mM in acetonitrile) under stirring and was monitored UV-vis absorption. The solution was then transferred inside the glovebox into a suitable capillary EPR tube (for **[1]^0** and $[Ru(bpy)_2(dppz)]^+$) or a flat cell fitted with young valves (for **[1]$^+$**). Spectra were recorded at room temperature on a Bruker EMX X-band CW EPR spectrometer with a ER-4116 dual mode cavity (for **[1]^0** and $[Ru(bpy)_2(dppz)]^+$) or on a ER200D Bruker X-band CW EPR spectrometer with a ER-4104OR cavity (for **[1]$^+$**). Simulations were performed with the Matlab toolbox Easyspin. For **[1]$^+$**, initial isotropic hyperfine couplings were obtained with a DFT calculation on the oxo-dppqp ligand and optimized with the Easyspin function esfit.

Procedure for the photolysis of [1](PF$_6$)$_2$:

All the experiments were realized in a glovebox. All volume measurements and dilution were done using micropipettes. Experiments were carried out in 1 cm or 2 mm cuvette and monitored by UV-vis spectroscopy inside the glovebox. Irradiation was carried out with a 300W ozone-free Xe lamp (*Newport*) operated at 280 W, inside the glovebox (which is equipped with a specific quartz window), with the beam adjusted with a set of mirrors. The lamp was equipped with a 450 nm bandpass filter (see transmittance spectrum in Fig. S20) for the UV-visible monitoring and the quantum yield determination; for experiments requiring higher concentration in **[1](PF$_6$)$_2$** (EPR monitoring and ^{1}H NMR characterization), a 400 nm cut-on filter was employed together with a neutral density filter (0.3 o.d.), giving identical results. The irradiance E was measured inside the glovebox with a power-meter (Newport PM1918-R).

Experiments for UV-visible monitoring: A 1 cm cuvette was filled with 2.7 mL of a 167 mM solution of TEA in dry degassed acetonitrile. After the blank measurement in the dark, 0.3 mL of a 150 µM stock solution of complex **[1](PF$_6$)$_2$** in dry and degassed acetonitrile was added and the resulting 15 µM solution was irradiated inside the glovebox. The spectral evolution was monitored by UV-vis spectroscopy.

Experiments for quantum yield determination: A 1 cm cuvette was filled with 1.9 mL of dry degassed acetonitrile and 43 µL of TEA (final concentration in 2 mL: 0.15 M). After the blank measurement in the dark, 57 µL of a 532 µM stock solution of complex **[1](PF$_6$)$_2$** in dry and degassed acetonitrile was added and the resulting 15 µM solution was irradiated inside the glovebox, using a cuvette holder with a beam impact area of 1 cm^2 (area fixed using black sellotape). The spectral evolution was monitored by UV-vis spectroscopy. Details regarding the quantum yield determination are given in Figure S20.

Experiments for ^{1}H NMR characterization: A 2 mm light path cuvette was filled with 500 µL of a 0.25 mM solution of complex **[1](PF$_6$)$_2$** in dry degassed CD_3CN. After recording a reference spectrum, 10 µL of TEA were added (final concentration in 510 µL: 143 mM) and the solution was irradiated inside the glovebox. The spectral evolution was monitored by UV-vis spectroscopy. When the reaction was completed, the solution was transferred in a specific NMR tube closed with a young valve for ^{1}H NMR spectroscopy characterization.

Experiments for EPR monitoring: A 2 mm cuvette was filled with 0.415 mL of a 200 µM solution of complex **[1](PF$_6$)$_2$** in a mixture of dry and degassed acetonitrile and propionitrile (1:2). 15 µL of TEA was then added (0.25 M) in the dark and the sample was irradiated inside the glovebox. The spectral evolution was monitored by UV-vis spectroscopy. The solution was then transferred to a suitable capillary EPR tube, sealed in the glovebox before its handling to the EPR spectrometer.

Procedure for UV/Vis- and rR-Spectroelectrochemistry:

For spectroelectrochemical (SEC) measurements, the sample (concentrations for UV/Vis-SEC: 0.1 mM **[1](PF$_6$)$_2$**, 0.1 mM [Ru(bpy)$_2$(dppz)](PF$_6$)$_2$; for rR-SEC: 0.1 mM **[1](PF$_6$)$_2$**, 0.1 mM [Ru(bpy)$_2$(dppz)](PF$_6$)$_2$) was dissolved in water-free acetonitrile containing 0.1 M tetrabutylammonium tetrafluoroborate (Sigma–Aldrich, for electrochemical analysis, +99.0%) as supporting electrolyte. Acetonitrile (Sigma–Aldrich, spectroscopic grade) was dried using calcium hydride (Sigma–Aldrich, 95%), distilled twice and kept under an argon atmosphere. All solutions were degassed with argon prior to each spectroelectrochemical measurement. SEC measurements were performed in a thin-layer quartz glass SEC cell (1 mm path length, Bioanalytical Systems). The

cell was equipped with a platinum mesh working electrode, a platinum wire counter electrode, and an Ag/AgCl pseudo-reference electrode. Cyclic voltammetry and chronoamperometry were performed using a VersaSTAT 3 (Princeton Applied Research) potentiostat. Singly-oxidized, singly-reduced and doubly reduced $\mathbf{[1]^{2+}}$ was generated by controlled potential electrolysis while UV/Vis- and rR spectra were detected, respectively. The UV/Vis-spectra were collected in transmission using a Cary 5000 UV/Vis spectrophotometer (Varian, USA). The rR measurements were performed with a 180° scattering arrangement. Using a 10x microscope objective (Olympus) the laser light (λ=458 nm, argon ion laser: Innova 300C, Coherent, USA) was focused into one of the holes of the platinum-mesh working electrode. The resonance Raman signal was detected by an Acton SpectraPro 2750 spectrometer (entrance slit width 100 mm, focal length 750 mm, grating 1800mm^{-1}) and a liquid nitrogen-cooled CCD camera (Princeton Instruments).

Computational Details

Calculations on $\mathbf{[1]^{2+}}$, $\mathbf{[1]^{+}}$ and $\mathbf{[1]^{0}}$ were performed using Gaussian 09.[2] Fully relaxed equilibrium structures for $\mathbf{[1]^{2+}}$ (singlet), $\mathbf{[1]^{+}}$ (doublet) and $\mathbf{[1]^{0}}$ (singlet and triplet) were obtained at the density functional level of theory (DFT), using the exchange correlation hybrid functional B3LYP[3] (VWN3) in combination with the MWB electronic core potential for 28 electrons and the respective double-ζ basis set for ruthenium[4] as well as the 6-31G(d) double-ζ basis set[5] for the main group elements. Solvent effects were included by the integral equation formalism of the polarizable continuum model (IEFPCM)[6] for acetonitrile. Subsequent vibrational analyses were performed for all optimized geometries revealing (local) minima on the potential energy surfaces. Time-dependent DFT (TDDFT) simulations on the 100 lowest excited states were carried out for all investigated redox states, while the same computational setup as for the preliminary ground state calculations was applied. Calculations with respect to the π-stacked dimers of $\mathbf{[1]^{2+}}$ were conducted using ORCA[7] at the DFT

[2] Gaussian 09, Revision A.02, M. J. Frisch, G. W. Trucks, H. B. Schlegel, G. E. Scuseria, M. A. Robb, J. R. Cheeseman, G. Scalmani, V. Barone, G. A. Petersson, H. Nakatsuji, X. Li, M. Caricato, A. Marenich, J. Bloino, B. G. Janesko, R. Gomperts, B. Mennucci, H. P. Hratchian, J. V. Ortiz, A. F. Izmaylov, J. L. Sonnenberg, D. Williams-Young, F. Ding, F. Lipparini, F. Egidi, J. Goings, B. Peng, A. Petrone, T. Henderson, D. Ranasinghe, V. G. Zakrzewski, J. Gao, N. Rega, G. Zheng, W. Liang, M. Hada, M. Ehara, K. Toyota, R. Fukuda, J. Hasegawa, M. Ishida, T. Nakajima, Y. Honda, O. Kitao, H. Nakai, T. Vreven, K. Throssell, J. A. Montgomery, Jr., J. E. Peralta, F. Ogliaro, M. Bearpark, J. J. Heyd, E. Brothers, K. N. Kudin, V. N. Staroverov, T. Keith, R. Kobayashi, J. Normand, K. Raghavachari, A. Rendell, J. C. Burant, S. S. Iyengar, J. Tomasi, M. Cossi, J. M. Millam, M. Klene, C. Adamo, R. Cammi, J. W. Ochterski, R. L. Martin, K. Morokuma, O. Farkas, J. B. Foresman, and D. J. Fox, Gaussian, Inc., Wallingford CT, 2016.

[3] a) A. D. Becke, *J. Chem. Phys*. **1993**, *98*, 5648; b) A. D. Becke, *Phys. Rev. A* **1988**, *38*, 3098; c) S. H. Vosko, , L. Wilk, and M. Nusair, *Canadian Journal of Physics*, **1980**, *58* (8): 1200-1211; d) P. J. Stephens, F. J. Devlin, C. F. Chabalowski, M. J. Frisch, *J. Phys. Chem*., **1994**, *98* (45), pp 11623–11627 ; e) Lee, C.; Yang, W.; Parr, R. G. *Phys Rev B* **1988**, *37*, 785–789.

[4] Andrae, D., Häußermann, U., Dolg, M. et al. *Theoret. Chim. Acta* **1990**, *77* (2), 123-141.

[5] Hariharan, P.C. and Pople, J.A. *Theoret. Chim. Acta* **1973**, *28* (3), 213-222.

[6] B. Mennucci, C. Cappelli, C. A. Guido, R. Cammi and J. Tomasi, *J. Phys. Chem. A*, **2009**, *113* (13), pp 3009–3020.

[7] ORCA 4.0.1.2 a) F. Neese, *WIREs Comput Mol Sci* **2012**, *2* (1), 73-78; b) F. Neese, *WIREs Comput Mol Sci* **2017**,

level of theory using the B3LYP (VWN5) hybrid functional. Atom-pairwise dispersion correction using the Becke-Johnson damping (D3BJ)[8] was applied to describe noncovalent interactions between the monomers. For all atoms, Ahlrichs' double-ζ basis set def2-SVP[9] was applied, which treats ruthenium with the Stuttgart def2-ECP.[10] Solvent effects were included as single point calculations on top of the optimized geometries, using the conductor like continuum model (CPCM)[11] for acetonitrile. The π-stacking distances were obtained by orthogonal regression of two parallel planes through the dppqp-ligands by minimizing the following sum:

$$\sum_{i=1}^{N} \frac{z_{1,i} - (m\,x_{1,i} + n\,y_{1,i} + t_1)^2}{1 + m^2 + n^2} + \sum_{i=1}^{N} \frac{z_{2,i} - (m\,x_{2,i} + n\,y_{2,i} + t_2)^2}{1 + m^2 + n^2} \quad ,$$

the distance *d* between the respective planes is then defined as:

$$d = \frac{t_2 - t_1}{\sqrt{1 + m^2 + n^2}} \quad .$$

e1327.

[8] a) S. Grimme, S. Ehrlich, L. Goerigk, *J. Comput. Chem*. **2011**, *32*, 1456-1465 b) S. Grimme, J. Antony, S. Ehrlich, H. Krieg, *J. Chem. Phys*. **2010**, *132*, 154104.

[9] F. Weigend and R. Ahlrichs, *Phys. Chem. Chem. Phys*. **2005**, *7*, 3297.

[10] D. Andrae, U. Häußermann, M. Dolg, H. Stoll, H. Preuß, *Theor. Chim. Acta* **1990**, *77*, 123-142.

[11] V. Barone, M. Cossi, *J. Phys. Chem. A*, **1998**, *102*, 1995.

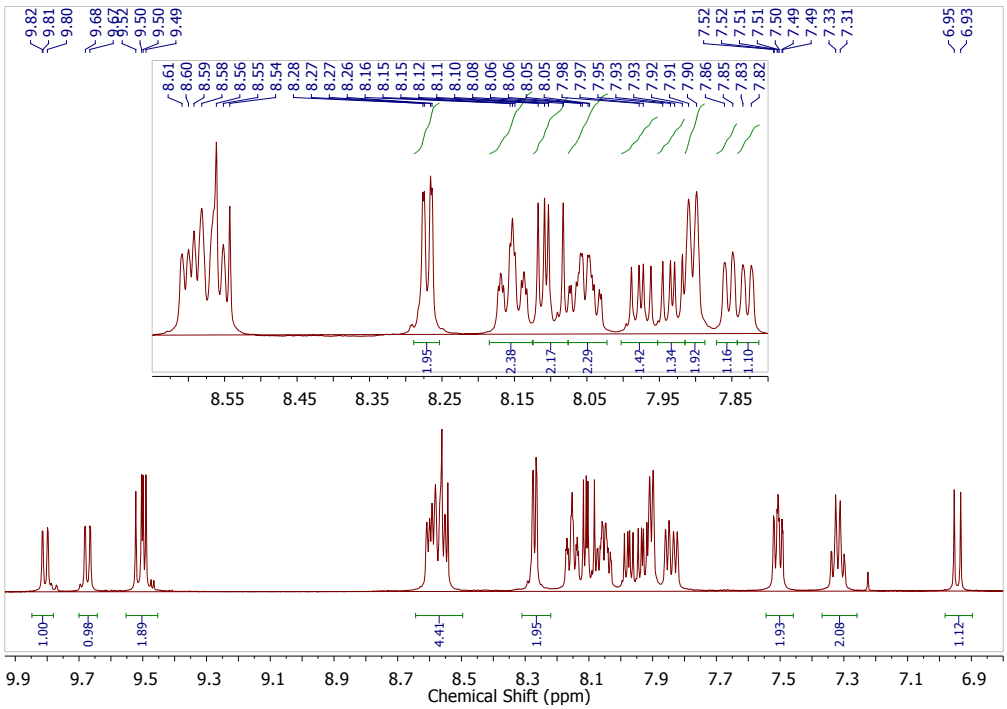

Figure S1. ^{1}H NMR spectrum of complex **[1](PF$_6$)$_2$** at 5·10^{-3} M in CD_3CN (500 MHz, 25°C).

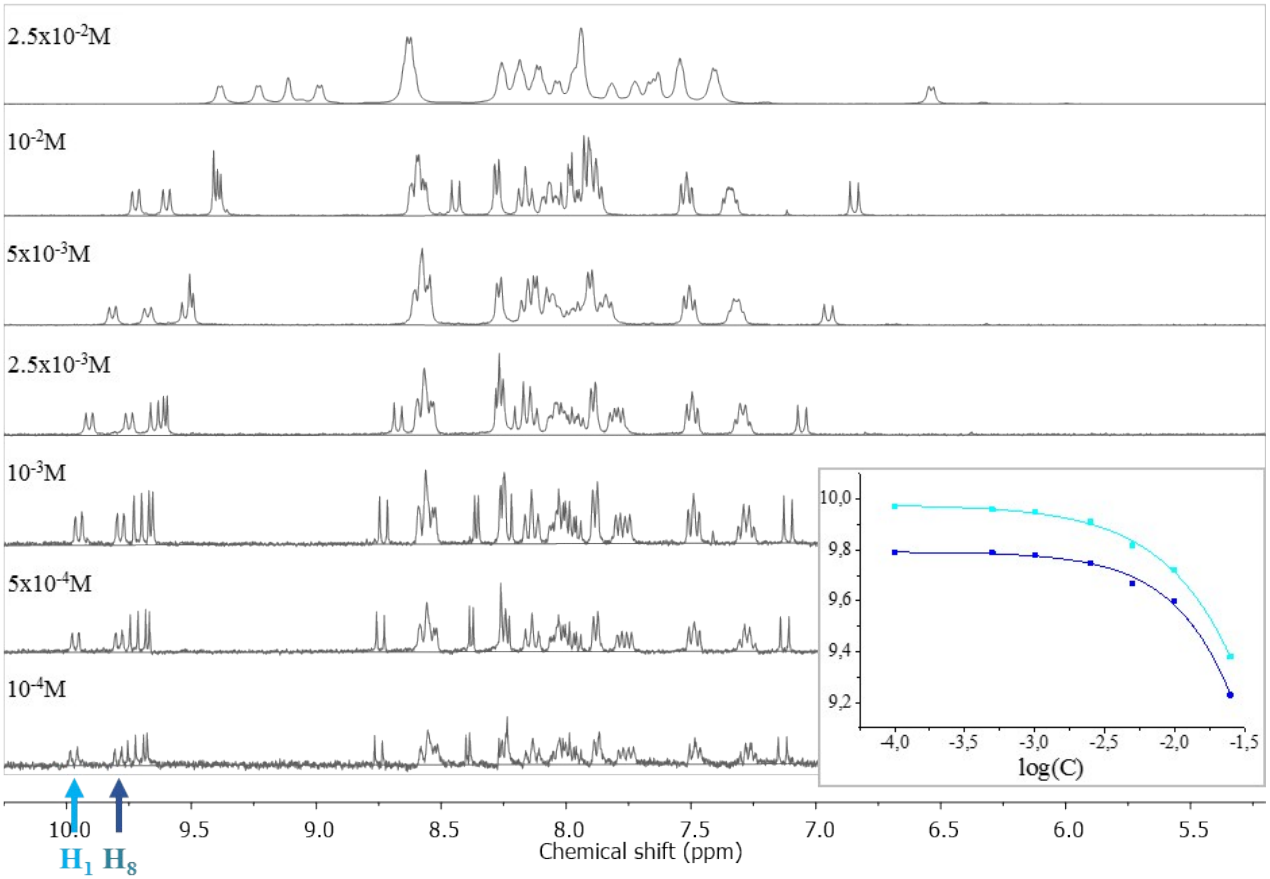

Figure S2. ^{1}H NMR spectra of complex **[1](PF$_6$)$_2$** at different concentrations from 10^{-4} to 2.5·10^{-2} M in CD_3CN; Inset: δ = log(C) for H_1 and H_8.

The curve of the chemical shift versus log(C) displays a plateau at low concentrations, where the monomer is sole present in solution, and an intermediate concentration range where monomer **[1]$^{2+}$**

and π-π stacked dimer $\{[\mathbf{1}]_2\}^{4+}$ coexist in solution. Due to the limited solubility of $[Ru(bpy)_2(oxo\text{-}dppqp)](PF_6)_2$, the expected second plateau at high concentrations, where the dimerization equilibrium is fully displaced in favor of $\{[\mathbf{1}]_2\}^{4+}$ could not be observed. The limit concentration for the existence of the sole monomer $[\mathbf{1}]^{2+}$ in solution is estimated to $5 \cdot 10^{-4}$ M and was taken into consideration for the following spectroscopic and electrochemical measurements.

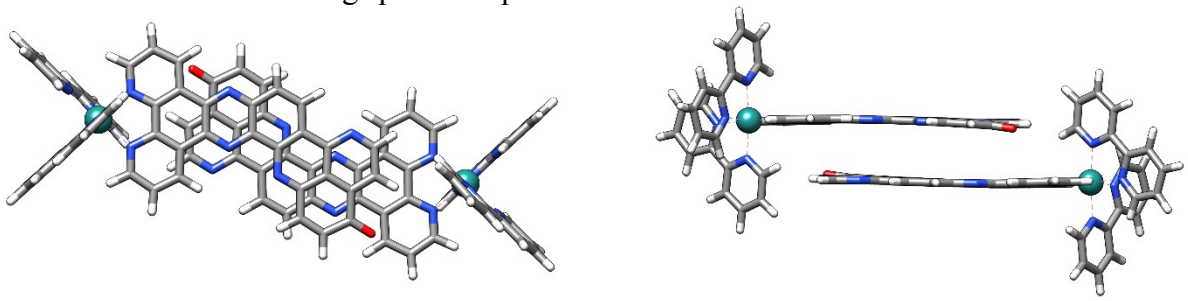

Figure S3. Optimized equilibrium structure of the *π*–stacked dimer, exemplarily shown for $\{[\mathbf{1}]_2\}^{4+}$ (dimer of $[\mathbf{1}]^{2+}$). (left) Arrangement of overlapping oxo-dppqp ligands displaced by half a ring; (right) π–stacking distance and slight loss of planarity upon aggregation.

Table S1. π–stacking distances (*d*) and bonding energies (E_{dimer}) for $\{[\mathbf{1}]_2\}^{4+}$, $\{[\mathbf{1}]_2\}^{2+}$ and $\{[\mathbf{1}]_2\}^{0}$ (dimers of $[\mathbf{1}]^{2+}$, $[\mathbf{1}]^{+}$ and $[\mathbf{1}]^{0}$). B3LYP-D3BJ/def2-SVP/CPCM(ACN)//B3LYP-D3BJ/def2-SVP

Dimer	Spin	*d* / Å	E_{dimer} / kJ/mol
$\{[\mathbf{1}]_2\}^{4+}$	Singlet	3.17	-132 (2x $^1[1]^{2+}$)
$\{[\mathbf{1}]_2\}^{2+}$	Singlet	3.03	-183 (2x $^2[1]^{+}$) -251 ($^1[1]^{2+}$ + $^1[1]^0$)
	Triplet	3.08	-160 (2x $^2[1]^{+}$) -230 ($^1[1]^{2+}$ + $^3[1]^0$)
$\{[\mathbf{1}]_2\}^{0}$	Singlet	3.03	-117 (2x $^1[1]^0$) -251 (2x $^3[1]^0$)
	Triplet	3.02	-141 ($^1[1]^0$ + $^3[1]^0$)
	Quintet	3.18	-160 (2x $^3[1]^0$)

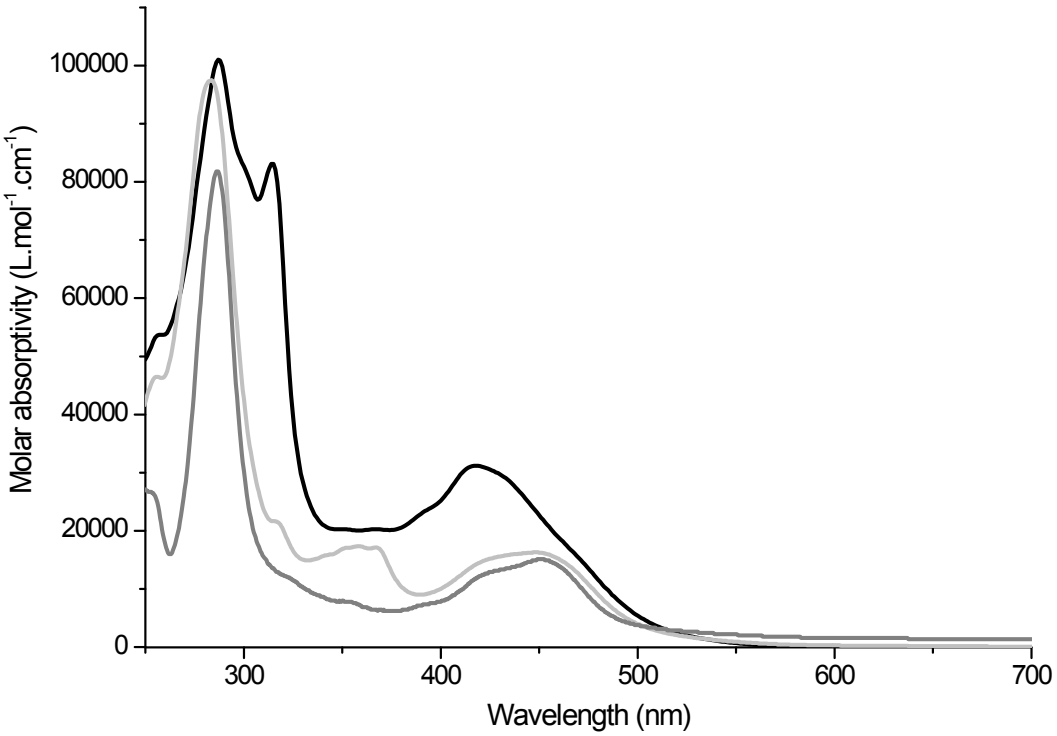

Figure S4. UV/Visible spectra of $[Ru(bpy)_2(dppz)](PF_6)_2$ (grey), $[Ru(bpy)_3](PF_6)_2$ (dark grey) and **[1](PF$_6$)$_2$** (black) in acetonitrile.

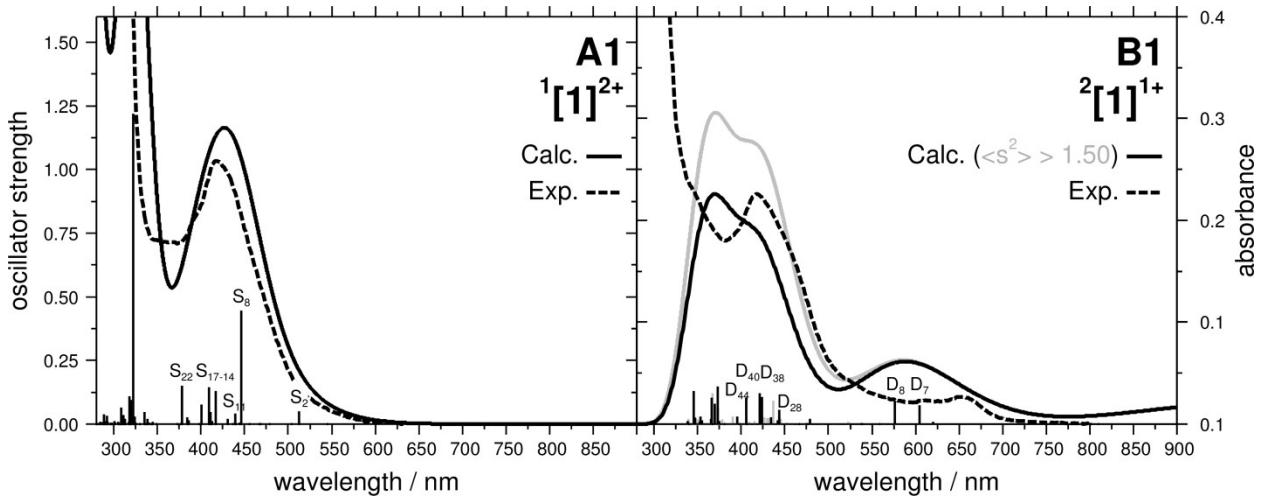

State	Hole / Electron	λ / nm	f	State	Hole / Electron	λ / nm	f
S_2	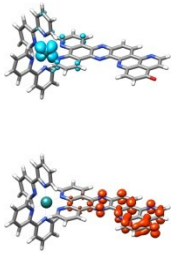	512	0.05	D_7	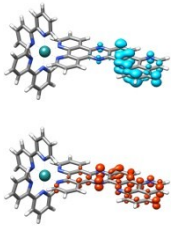	605	0.07
S_8	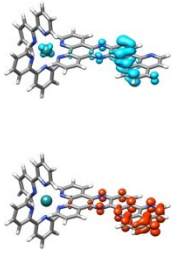	446	0.44	D_8	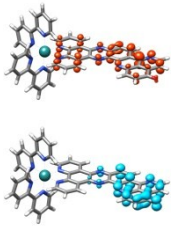	576	0.09
S_{11}	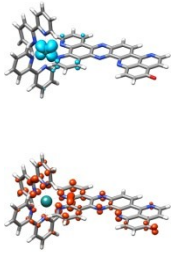	439	0.04	D_{28}	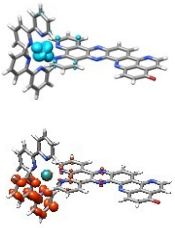	444	0.06
S_{14}	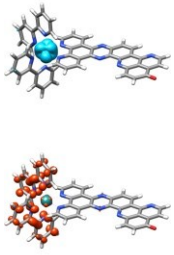	411	0.05	D_{38}	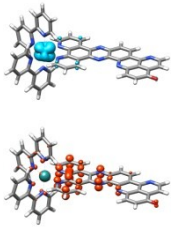	424	0.11

S_{16}	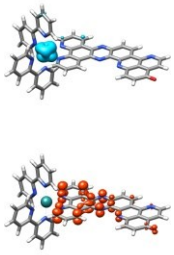	417	0.13	D_{40}	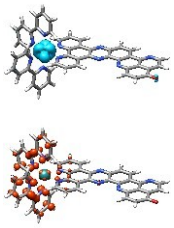	421	0.12
S_{17}	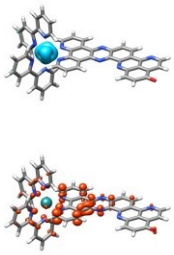	409	0.14	D_{44}	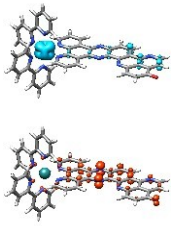	405	0.10
S_{18}	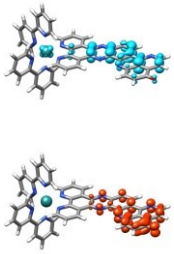	400	0.08	D_{44}	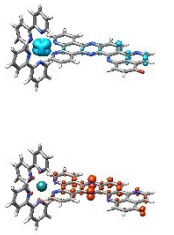	405	0.10
S_{22}	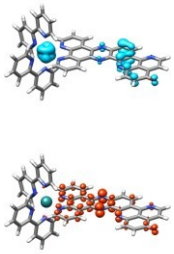	378	0.15				

Figure S5. Simulated UV visible absorption spectra of **[1]**$^{2+}$[12] (A1) and **[1]**$^{+}$ (B1). Calculated vertical transitions and oscillator strengths are presented by bars. For the transitions of **[1]**$^{+}$ (doublet multiplicity, unrestricted calculation) eigenvalues of the total spin-squared operator $\langle S^2 \rangle$ are indicated by color (see inset). A Gaussian function with a full-width at half-maximum (fwhm) of 0.28 eV was employed to broaden the transitions in the simulated spectrum. Selected transitions of the bright states within the visible region of **[1]**$^{2+}$ and **[1]**$^{+}$ are visualized (charge density: from blue to red) in A2 and B2, respectively.

[12] J. Schindler , Y. Zhang, P. Traber, J.-F. Lefebvre, S. Kupfer, M. Demeunynck, S. Grafe, M. Chavarot-Kerlidou and B. Dietzek *Submitted for publication*.

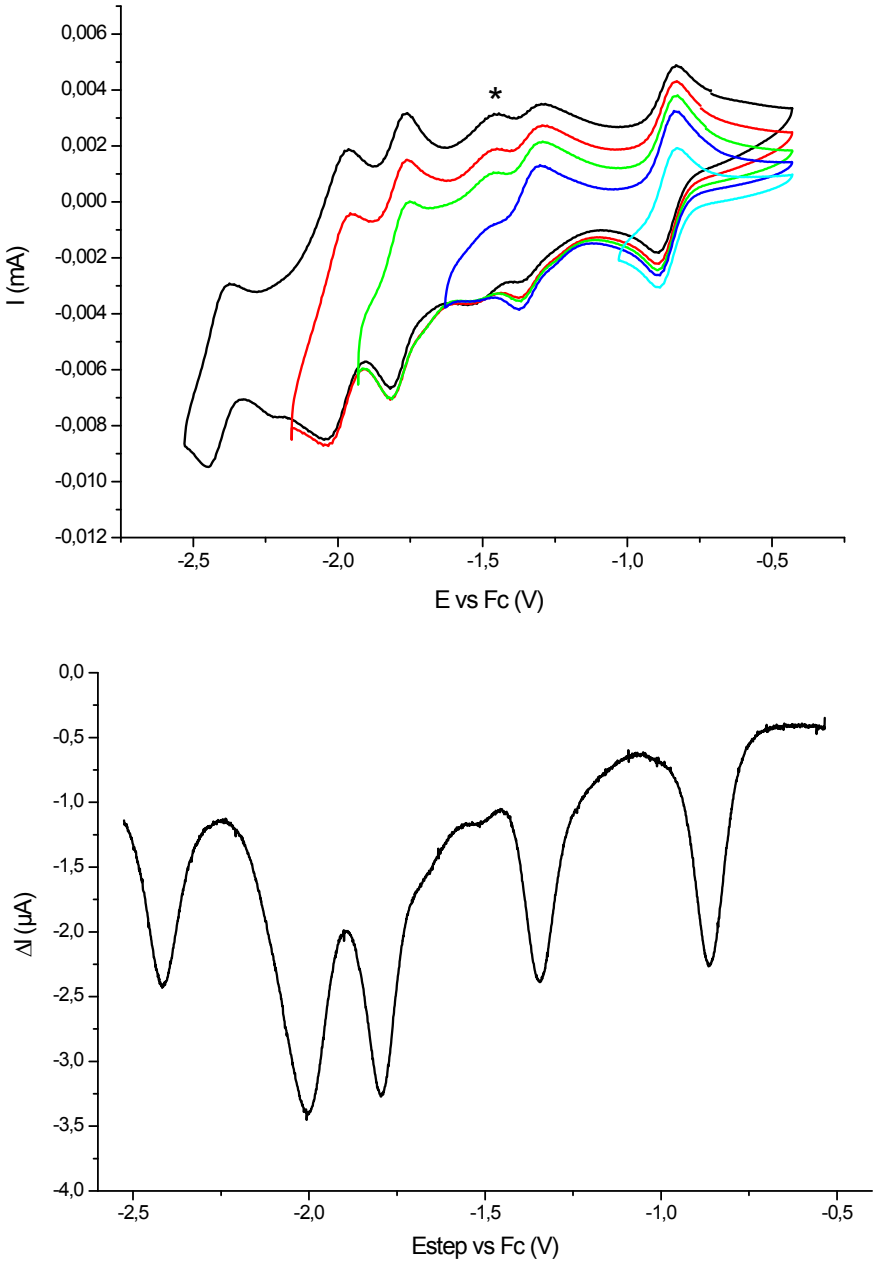

Figure S6. Cyclic (top, 100 mV.s^{-1}) and differential pulse (cathodic scan; bottom) voltammograms of **[1](PF$_6$)$_2$ (**0.25 mM**)** recorded on a glassy carbon electrode in a 0.1 M TBAPF$_6$ solution in DMF. (DPV parameters: P_{Height} = 10 mV, P_{Width} = 50 ms, S_{Height} = -1 mV, S_T = 200 ms).
* The labelled wave is assigned to reoxidation of some π–stacked complex formed upon reduction, as stacking is calculated to be favored upon reduction (see Table S1).

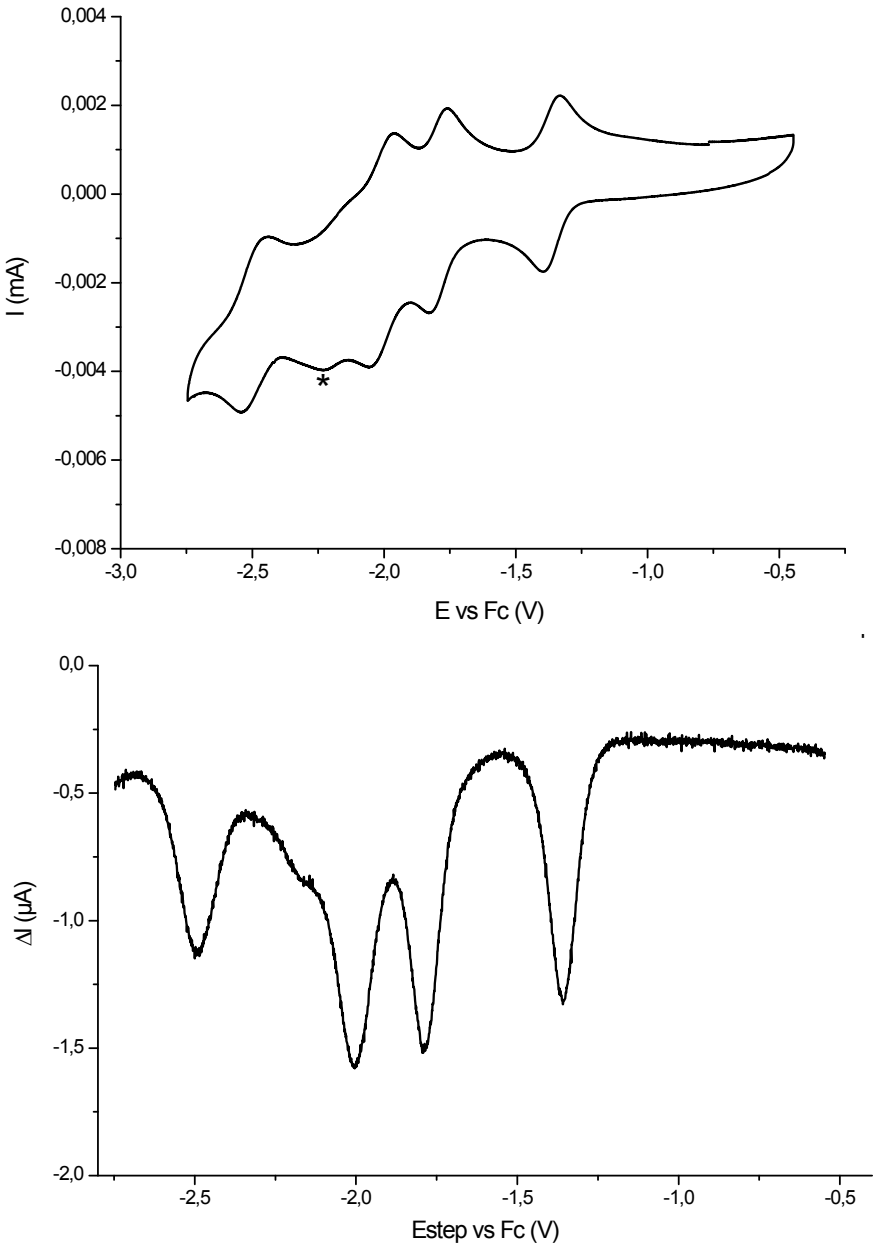

Figure S7. Cyclic (top) and differential pulse (cathodic scan; bottom) voltammograms of complex $[Ru(bpy)_2(dppz)](PF_6)_2$ **(**0.5 mM**)** recorded on a glassy carbon electrode in a 0.1M $TBAPF_6$ solution in DMF. (DPV parameters: P_{Height} = 10 mV, P_{Width} = 50 ms, S_{Height} = -1 mV, S_T = 200 ms).
* The labelled wave is assigned to reduction of some π–stacked complex formed upon reduction.

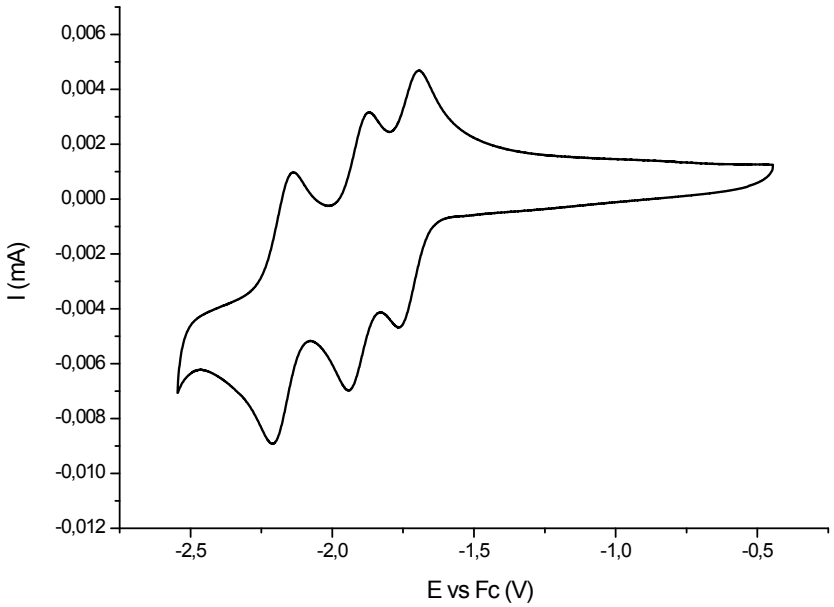

Figure S8. Cyclic voltammogram of complex $[Ru(bpy)_3](PF_6)_2$ (1 mM) recorded on a glassy carbon electrode in a 0.1 M $TBAPF_6$ solution in DMF.

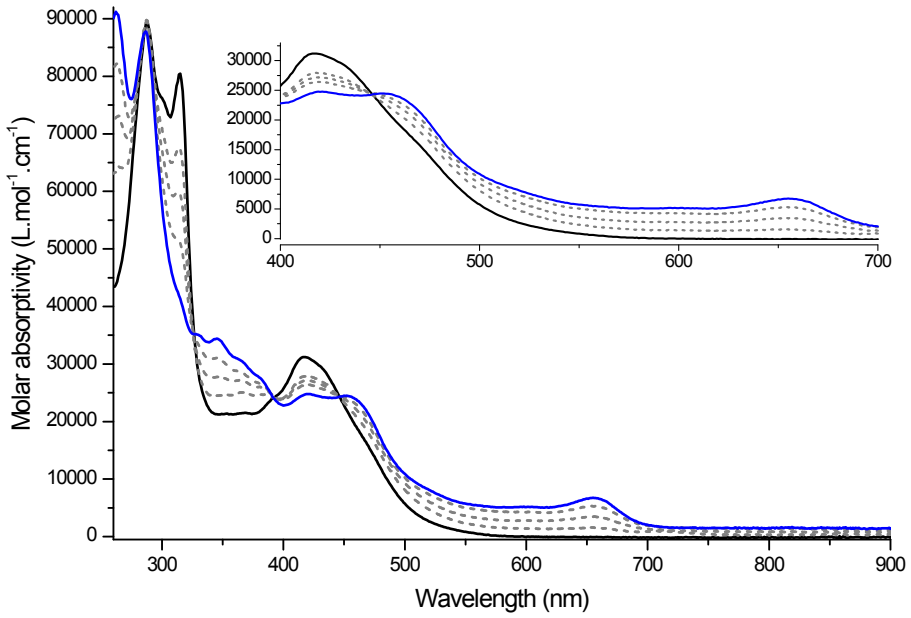

Figure S9. UV/Visible absorption monitoring of the chemical reduction of complex $\mathbf{[1]^{2+}}$ (15 µM in acetonitrile) by cobaltocene: formation of the singly-reduced species $\mathbf{[1]^{1+}}$ (blue).
The one-electron reduction was completed after addition of 1.35 eq. of Cp_2Co (0.35 eq. of reducing agent are consumed to quench residual traces of O_2).

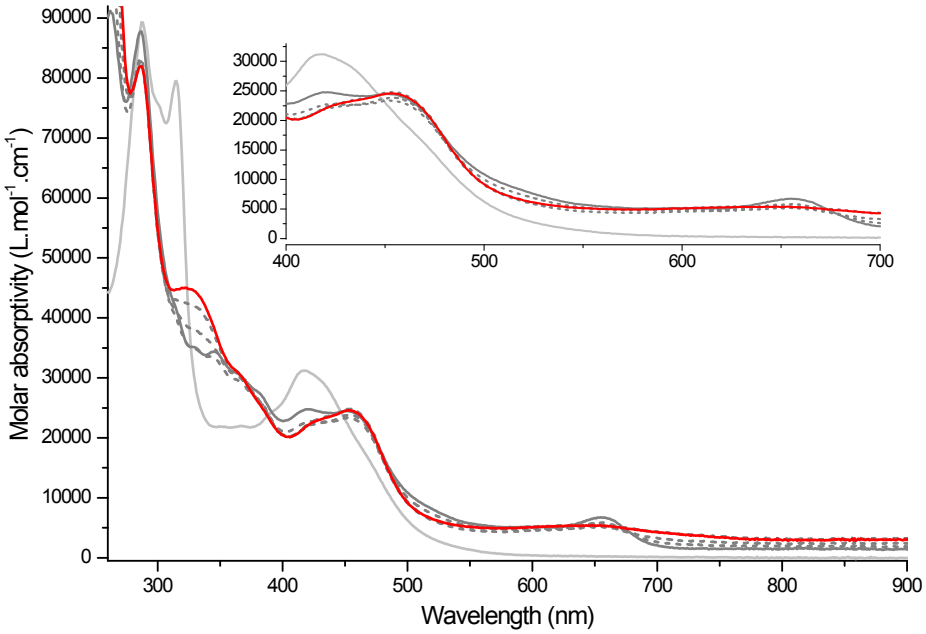

Figure S10. UV/Visible absorption monitoring of the chemical reduction of complex $\mathbf{[1]^{2+}}$ (15 µM in acetonitrile) by cobaltocene: formation of the doubly-reduced species $\mathbf{[1]^{0}}$ (red). Indicated in grey: initial complex $\mathbf{[1]^{2+}}$; in dark grey: singly-reduced species $\mathbf{[1]^{+}}$.
1.08 supplementary equivalents of cobaltocene were added to the singly-reduced species (Fig. S14) to generate the doubly-reduced complex. Of note, addition of extra equivalents of cobaltocene didn't lead to any further change.

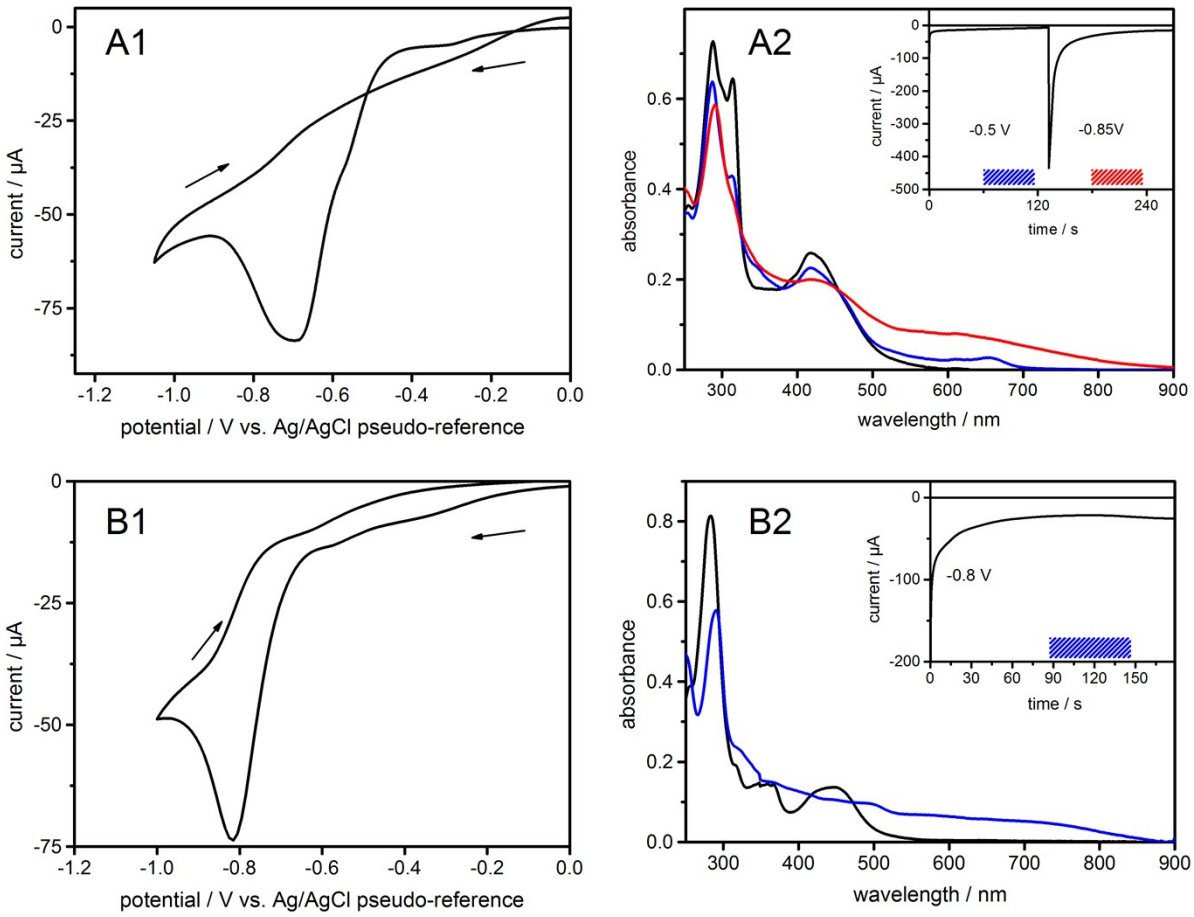

Figure S11: UV/Vis-spectroelectrochemical investigations in 0.1 M tetrabutylammonium tetrafluoroborate/acetonitrile. All potentials are measured against a Ag/AgCl pseudo-reference electrode.

Left: Cyclic voltammograms showing the first and second reduction process of $\mathbf{[1]^{2+}}$ (A1) as well as the first reduction process of $[Ru(bpy)_2(dppz)]^{2+}$ (B1).

Right: The absorption spectrum of $\mathbf{[1]^{2+}}$ (black line, A2) and $[Ru(bpy)_2(dppz)]^{2+}$ (black line, B2) are shown together with the absorption spectra observed during controlled potential electrolysis: singly-reduced $\mathbf{[1]^{2+}}$ (blue line, A2), doubly-reduced $\mathbf{[1]^{2+}}$ (red line, A2) and singly-reduced $[Ru(bpy)_2(dppz)]^{2+}$ (blue line, B2). The respective chronoamperograms are shown in the inset. The applied potential as well as the time necessary to collect each absorption spectrum is highlighted in each graph using the same color code.

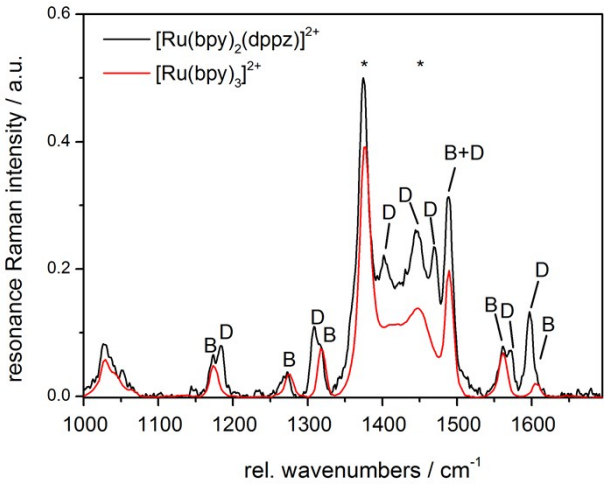

Fig. S12: rR spectrum of $[Ru(bpy)_2(dppz)]^{2+}$ in acetonitrile (black line, solvent bands indicated by an asterisk, excitation wavelength: 473 nm). rR bands characteristic for vibrations of the bpy (symbol B) and dppz ligand (symbol D) are indicated. Band assignment is based on comparison with the rR spectrum of $[Ru(bpy)_3]^{2+}$ (red line) and $[Ru(dppz)_3]^{2+}$.[13]

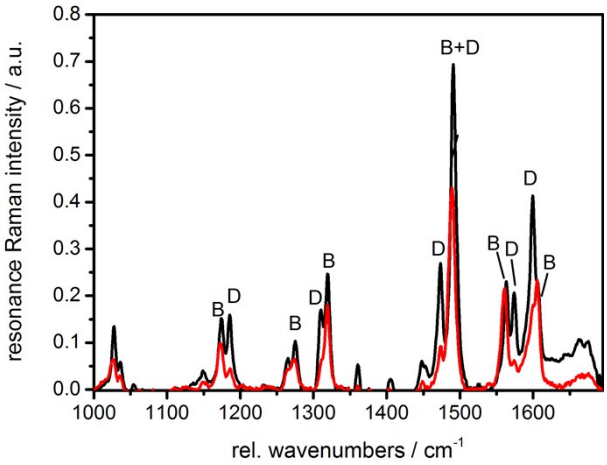

Fig. S13: rR spectrum of $[Ru(bpy)_2(dppz)]^{2+}$ (black) in comparison with the spectra collected during controlled potential electrolysis: first reduction (red; electrolysis at -0.85 V vs. Ag/AgCl pseudo-reference electrode) in 0.1 M tetrabutylammonium tetrafluoroborate/acetonitrile. rR spectra obtained upon excitation at 458 nm (solvent bands subtracted). rR bands characteristic for vibrations of the bpy (symbol B) and dppz ligand (symbol D) are indicated.

[13] C. G. Coates, L. Jacquet, J. J. McGarvey, S. E. Bell, A. H. Al-Obaidi and J. M. Kelly; *J. Am. Chem. Soc.*, **1997**, *119*, 7130-7136.

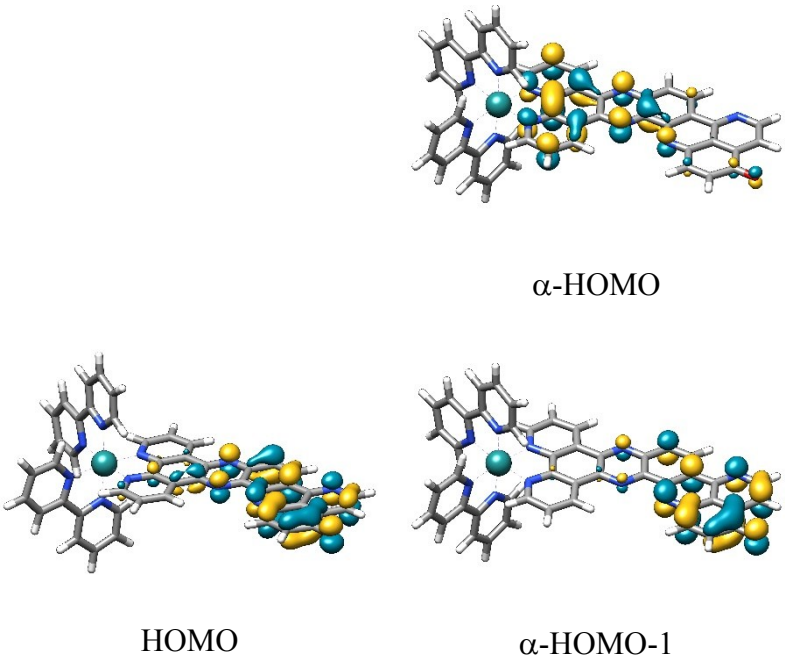

Figure S14. Calculated structures and frontier molecular orbitals carrying the excess charges in **[1]^{0}**: singlet state (left), triplet state (right).

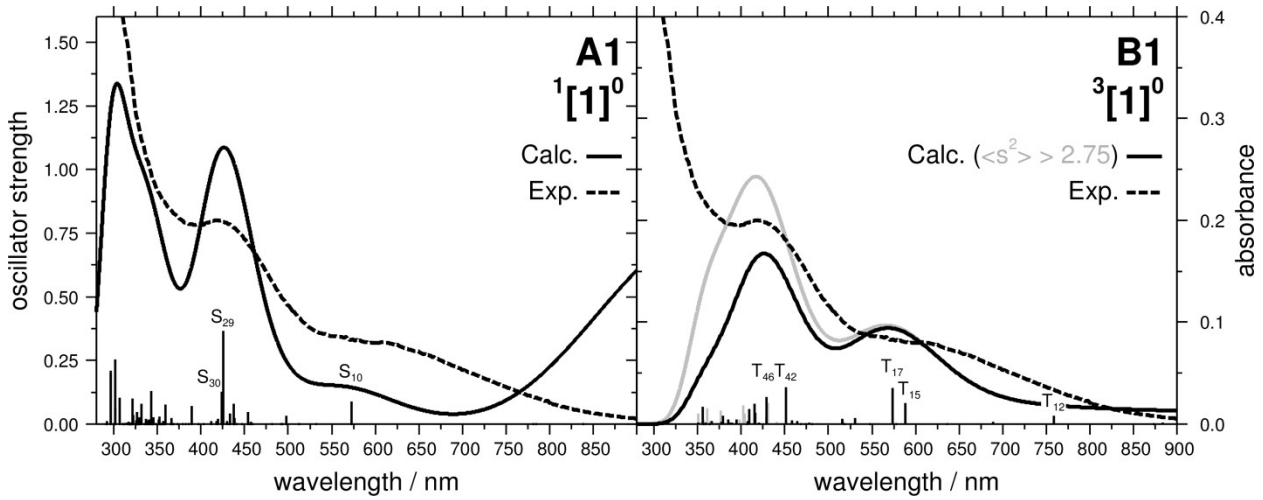

State	Hole / Electron	λ / nm	f
S_5	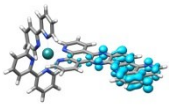	1027	0.49
S_6	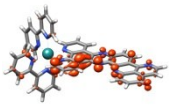	935	0.08
S_{10}	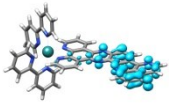	573	0.03
S_{29}	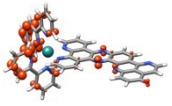	425	0.37

State	Hole / Electron	λ / nm	f
T_{12}	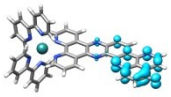	759	0.03
T_{15}	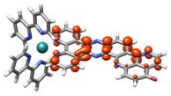	588	0.08
T_{17}	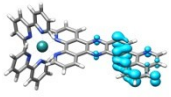	574	0.14
T_{42}	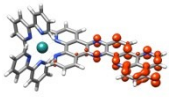	451	0.14

S_{30}	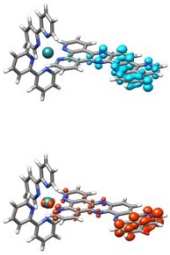	424	0.13	T_{46}	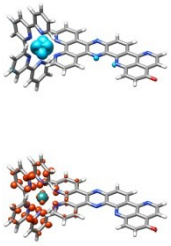	429	0.11

Figure S15. Simulated (solid) and experimental (dashed) UV visible absorption spectra of **[1]^0** in singlet (A1) and triplet (B1) multiplicity. Calculated vertical transitions and oscillator strengths are presented by bars. For the transitions of **^{3}[1]^0** (triplet multiplicity, unrestricted calculation), spin-contamination is indicated by $\langle S^2 \rangle$ (grey). A Gaussian function with a full-width at half-maximum (fwhm) of 0.28 eV was employed to broaden the transitions in the simulated spectrum. Selected transitions of the bright states within the visible region are visualized (charge density: from blue to red).

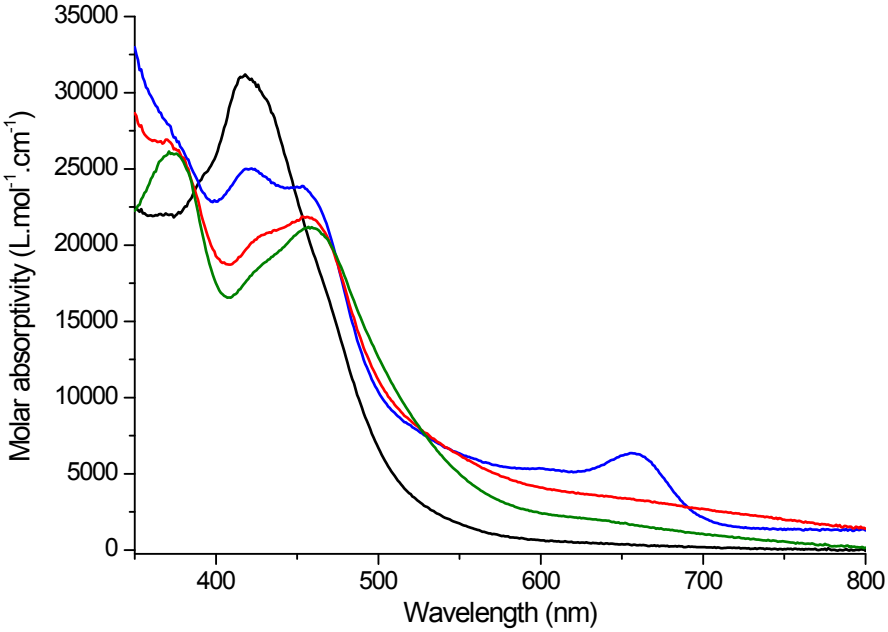

Figure S16. UV/Visible absorption spectra of $[\mathbf{1}]^{2+}$ (black), $[\mathbf{1}]^{+}$ (blue) $[\mathbf{1}]^{0}$ (red) and $[\mathbf{1H_2}]^{2+}$ (green) recorded at 200 µM in acetonitrile/propionitrile 1:2 (*EPR conditions*), using Cp_2Co as reducing agent and TFA as proton source. A 2 mm optical path cuvette was employed.

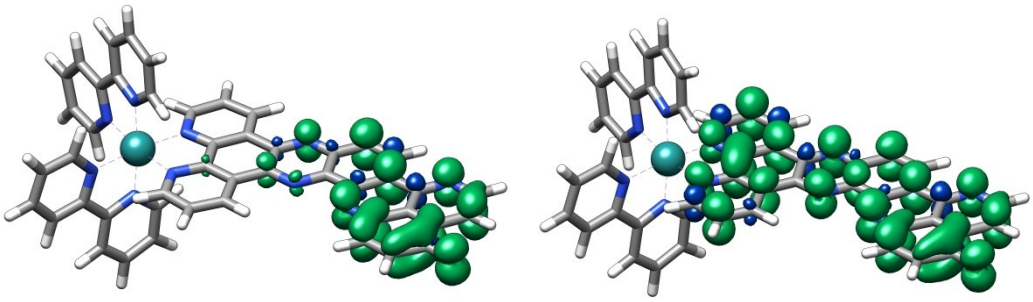

Figure S17: Spin density plots for $\mathbf{[1]^{1+}}$ (doublet) (left) and $\mathbf{[1]^{0}}$ (triplet state) (right).

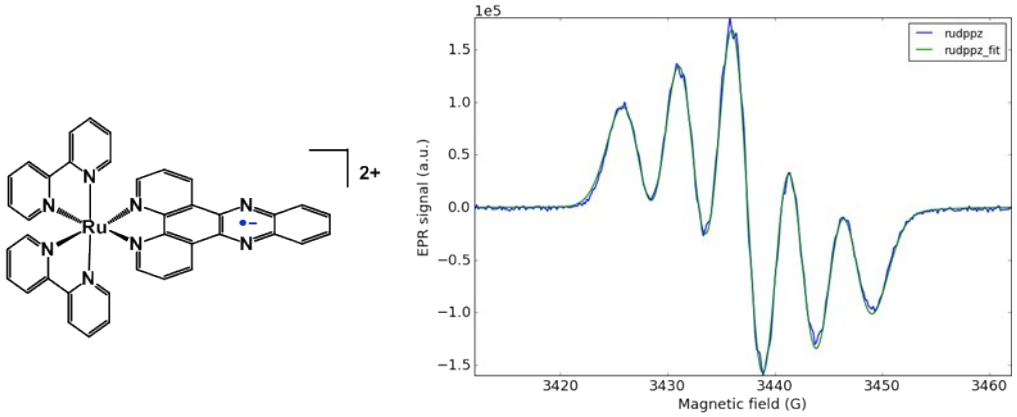

Fig. S18. X band EPR (blue) and simulated (green) spectra of the singly-reduced derivative of $[Ru(bpy)_2(dppz)](PF_6)_2$ (structure on the left).

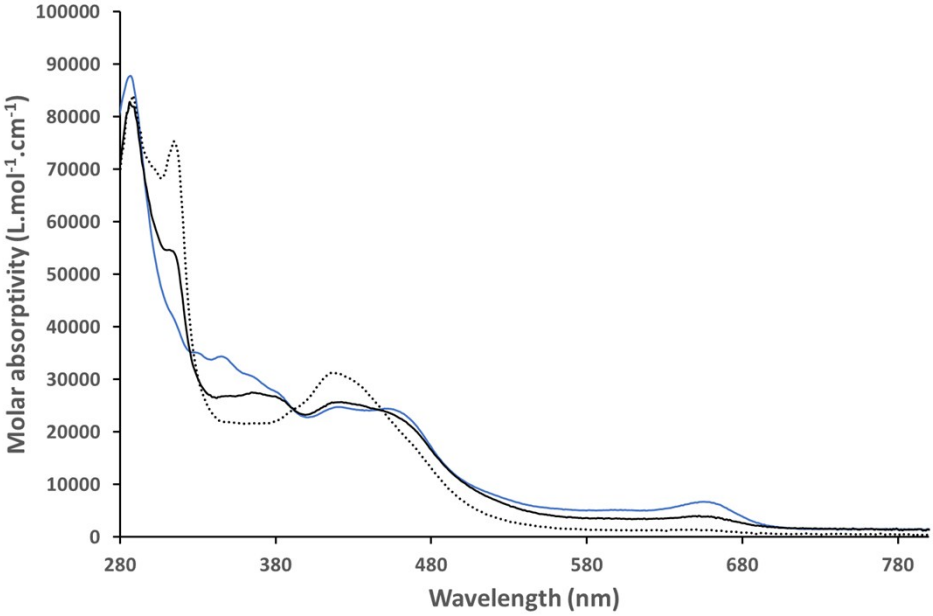

Figure S19. UV/Visible absorption monitoring of a photolysis experiment: (top) (bottom) spectrum recorded after 10s of photolysis (dark) compared to spectra of $[\mathbf{1}]^{2+}$ (dotted line) and $[\mathbf{1}]^{+}$ (blue).

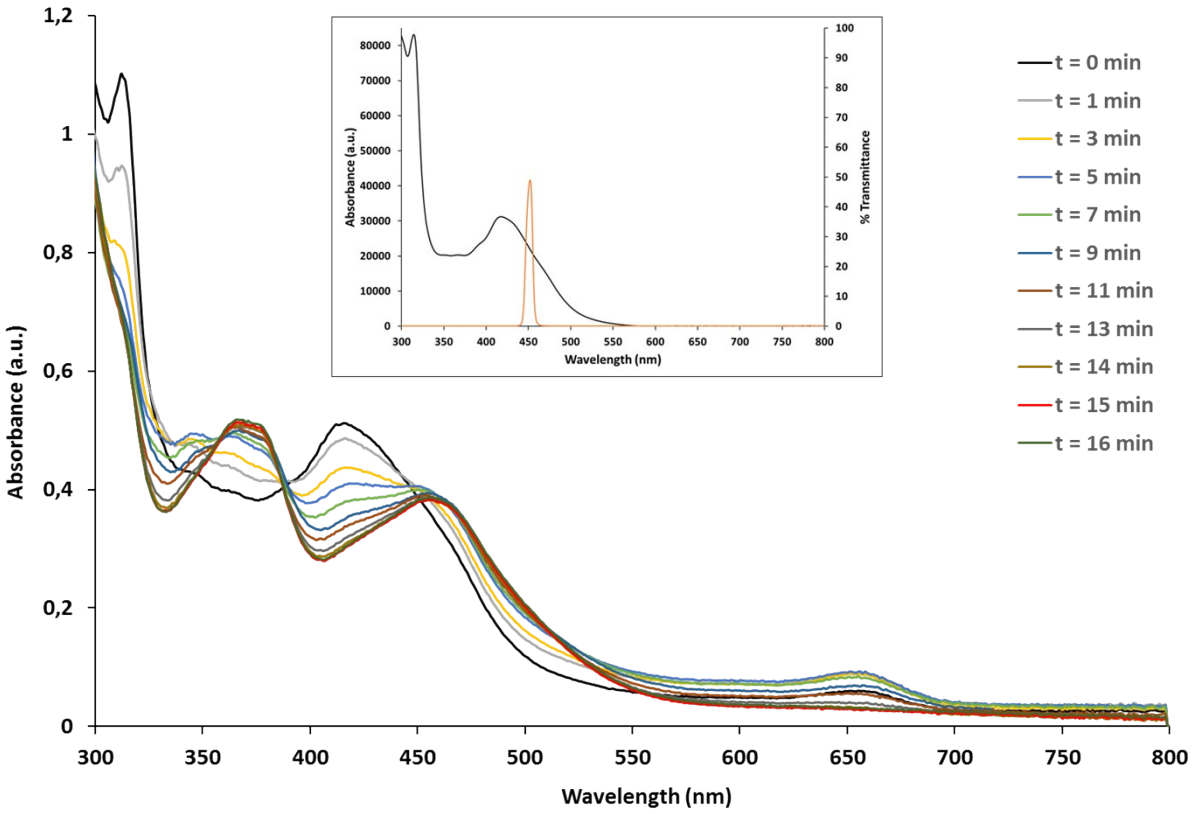

Figure S20. UV/Visible absorption monitoring of the photolysis experiment performed to determine the quantum yield. The photolysis of 2 mL of a 15 µM solution of **[1](PF$_6$)$_2$**, in the presence of 0.15 M of TEA in CH_3CN was completed after 15 min of irradiation (Absorption spectrum @ 16 min fully superimposable to the one @ 15 min). Inset: Superimposition of the absorption spectrum of **[1](PF$_6$)$_2$** (black) with the transmittance spectrum of the 450 nm band-pass filter used for the photolysis experiment.

Quantum yield determination:

An irradiance E of 45 µW.cm^{-2} was measured inside the glove-box. It was converted to the photon flux E_{QF} of 1.7 µE (1 Einstein = 1 mol.s^{-1}.m^{-2}) according to the following equation:

$$E_{QF} = E \text{ (in W.m}^{-2}\text{)} \times \lambda \text{ (in nm)} \times 5.03\ 10^{15} \text{ (in m}^{-2}\text{.s}^{-1}\text{)} / 6.02\ 10^{23} \text{ (in mol}^{-1}\text{)}$$

Taking into account the 1 cm^2 irradiation beam impact area and the 15 min reaction time required for full conversion of **[1]**$^{2+}$ into **[1H$_2$]**$^{2+}$, this corresponds to 152 nmol of photons fluxed during the course of the photolysis experiment, yielding 30 nmol of doubly-reduced doubly-protonnated complex (equivalent to 60 nmol of transferred electrons). This corresponds to a **40% quantum yield for two successive photoinduced electron transfers**, or 20% in case of a second dark reduction process by TEA$^{\bullet+}$ or another decomposition product of TEA. We nevertheless noticed that no evolution of the absorption spectrum was observed when the sample was left under stirring in the dark, after a few minutes of irradiation, this observation being in favour of a photodriven second electron transfer according to F. M. MacDonnell and coworkers, *Chem. Eur. J.* **2015**, *21*, 17314.

This quantum yield of 40% is however a lower limit value; it is, indeed, calculated based on the *number of incident photons* which are not all absorbed by the complex. At the beginning of the experiment, the absorbance of the solution at 450 nm is 0.402, which corresponds to a transmittance of 40% (A = log(1/T)). Thus, at start, only 60% of the incident photons are absorbed and account for the photolysis process. We can observe on Figure S20 that the absorbance value at 450 nm is roughly constant all along the experiment (slight decrease from 0.402 to 0.374); with the assumption that the transmittance is kept constant at 40% during the course of the experiment, we can estimate the number of absorbed photons: 152 nmol (incident photons) x 60% = 91 nmol (absorbed photons) and calculate **a *quantum yield of 66%, based on the amount of absorbed photons***.

It should also be noticed that, at high conversion, the final product $[\mathbf{1H_2}]^{2+}$ absorbs a substantial portion of the photons, leading to another underestimation of the quantum yield value. As suggested during the reviewing process, we tried to analyze the spectra recorded at early conversion, but without success. The relative intensities of the different absorption bands suggest that a mixture of reduced (singly, doubly) and protonated species are formed at an early stage of the photolysis; a complex deconvolution of the spectra is thus required to provide a quantitative data analysis.

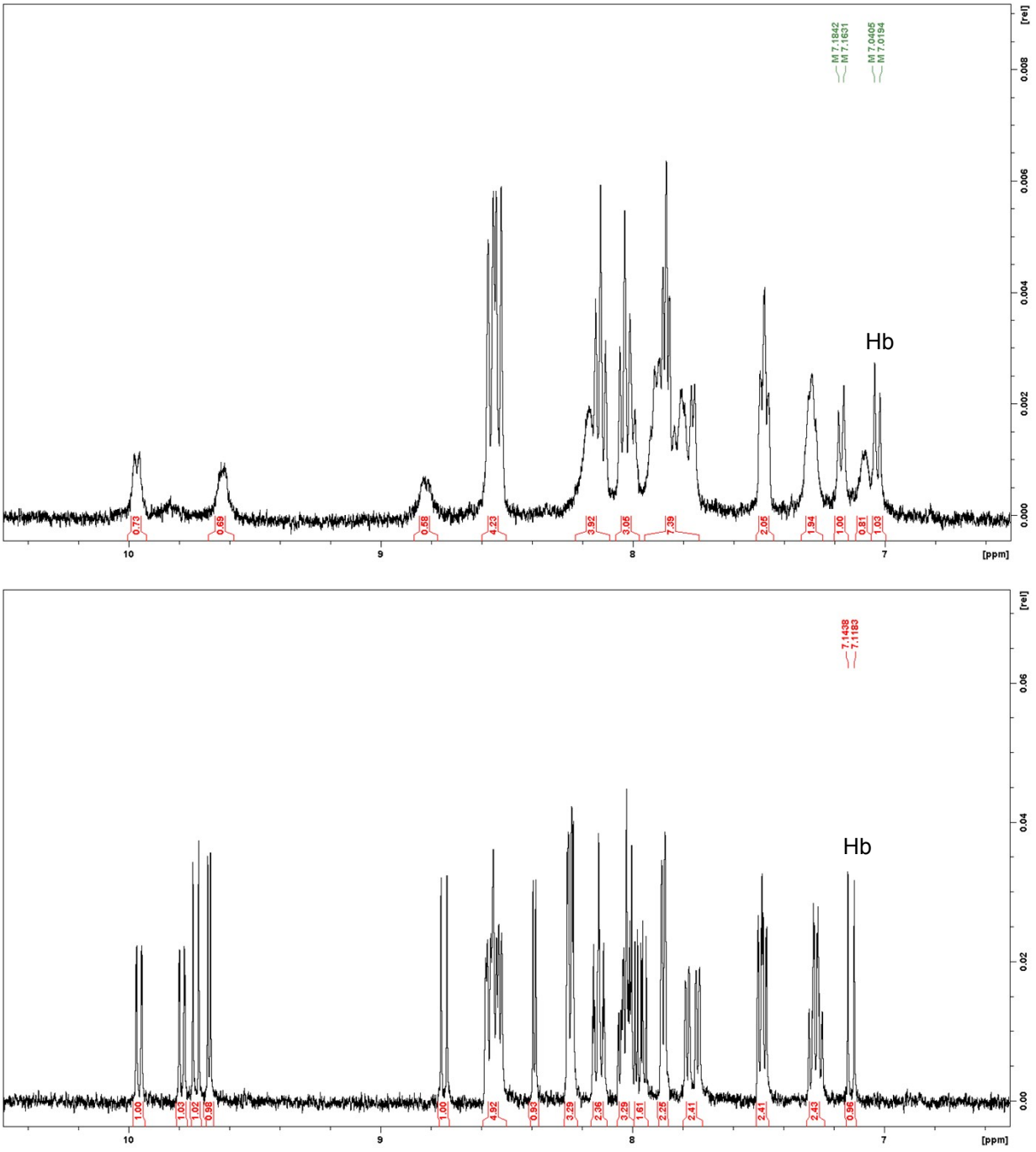

Figure S21. *Top*: ^{1}H NMR spectrum of the photolysis product, recorded at 400 MHz after irradiation of a 0.25 mM solution of **[1](PF$_6$)$_2$** in CD_3CN in presence of TEA. *Bottom*: Reference spectrum of **[1](PF$_6$)$_2$** (0.25 mM in CD_3CN, recorded on the same 400 MHz apparatus).

Two online tools, spinus web (http://www2.chemie.uni-erlangen.de/services/spinus/) and nmrdb (http://www.nmrdb.org/predictor/), were employed to predict the ^{1}H NMR modifications expected to occur upon conversion of $[\mathbf{1}]^{2+}$ into the doubly-reduced doubly-protonnated derivative $[\mathbf{1H_2}]^{2+}$.

We first checked the accuracy of their predictions using experimental ^{1}H NMR data, previously reported for a tetracyclic pyridoacridine (the design of the octacyclic oxo-dppqp ligand of complex

[1](PF$_6$)$_2$ is based on this previous work); a monoprotonated monomethylated methoxy pyridoacridine was used as model for the doubly protonated doubly reduced form of the iminobenzoquinone ligand. As shown in Table S2, both prediction tools give excellent correlations with these experimental data. *Moreover, one main difference observed between the ^{1}H NMR spectra of the pyridoacridone and the reduced methoxy-pyridoacridine form is the value of the coupling constant Jab for the Hb proton: due to the strong double-bond character in the iminobenzoquinone moiety, Jab is over 10 Hz in the oxidized form, compared to 8.5 Hz in the reduced form*.

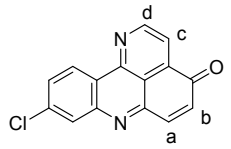

H position		a	b	c	d
Exp[1] (DMSO d6)	δ	7.87	6.96	8.19	9.41
	J	*10.3*	*10.3*	*4.6*	*4.6*
Spinus web	δ	7.9	6.9	7.7	9.0
	J	*10.2*	*10.2*	*5.0*	*5.0*
nmrdb	δ	7.9	6.9	7.7	9.1
	J	*10.2*	*10.2*	*5.0*	*5.0*

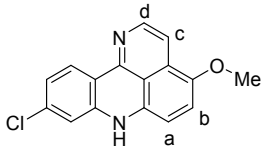

H position		a	b	c	d
Exp[2] ($CDCl_3$)	δ	6.73	7.15	7.28	8.16
	J	*8.5*	*8.5*	*6.0*	*6.0*
Spinus web	δ	6.8	7.1	7.6	8.4
	J	*8.7*	*8.7*	*5.4*	*5.4*
nmrdb	δ	7.0	7.2	7.8	8.4
	J	*8.6*	*8.6*	*5.4*	*5.4*

1. M. Demeunynck and coll. *Synthetic Commun*. **1997**, 2311.
2. M. Demeunynck and coll. *Magn. Resonance Chem*. **1997**, 697.

Table S2. Structure of the model pyridoacridine ligand in its oxidized (left) and reduced (right) forms, together with the comparison of the experimental ^{1}H NMR chemical shifts (δ) and coupling constants (*J*) for Ha, Hb, Hc, Hd with the predicted ones (using spinus web or nmrdb).

We then used these two prediction tools to calculate NMR data for the octacyclic ligand in its oxidized form (oxo-dppqp, bearing the iminobenzoquinone) and its doubly reduced doubly protonated form (aminophenol derivative). These data are listed in Table S3.

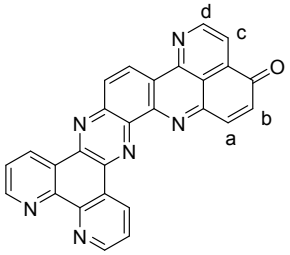

H position		a	**b**	c	d
Spinus web	δ	8.3	7.0	8.3	9.1
	J	*10.2*	***10.2***	*5.0*	*5.0*
nmrdb	δ	8.3	7.0	8.5	9.1
	J	*10.2*	***10.2***	*4.9*	*4.9*

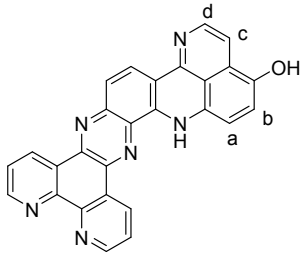

H position		a	**b**	c	d
Spinus web	δ	8.1	7.4	8.1	8.8
	J	*8.8*	***8.8***	*5.6*	*5.6*
nmrdb	δ	8.0	7.5	8.1	9.1
	J	*8.8*	***8.8***	*5.5*	*5.5*

Table S3. Structure of the oxo-dppqp ligand (left) and the doubly-reduced doubly-protonnated form (right), together with the predicted ^{1}H NMR chemical shifts (δ) and coupling constants (*J*).

As already observed with the tetracyclic pyridoacridine, the coupling constant *J*ab is highly characteristic of the oxidation state of the iminobenzoquinone part of the ligand (10.2 Hz for the

oxidized form versus 8.8 Hz for the reduced one). Importantly, unlike chemical shifts, this coupling constant is expected to be insensitive to "$Ru(bpy)_2$" complexation on the phen moiety, to medium (solvent, presence of excess TEA…) or to concentration (see Figure S2) effects. *It can therefore be used as probe of the chemical modification of the iminobenzoquinone moiety.*

Considering now the experimental ^1H NMR data (Figure S21) for **[1](PF$_6$)$_2$** recorded before photolysis, we clearly observe Hb at 7.13 ppm with ***J*ab = 10.2 Hz** in good agreement with the predictions. After photolysis, the Hb doublet is observed at 7.03 ppm with ***J*ab = 8.4 Hz**, in excellent agreement with the formation of a doubly-reduced doubly-protonnated complex during the photolysis experiment.

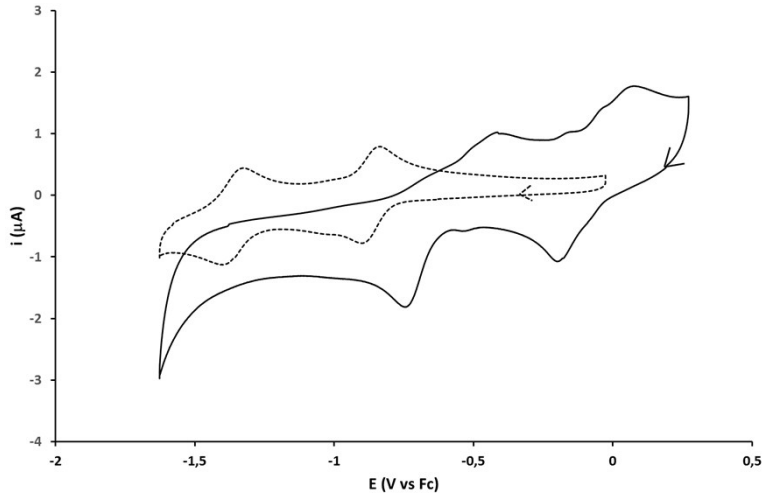

Figure S22. Cyclic voltammograms of **[1](PF$_6$)$_2$** recorded in the absence (dotted line) and in the presence (plain line) of excess trifluoroacetic acid (TFA), at a glassy carbon electrode in a 0.1 M n-Bu_4NPF_6 DMF solution.

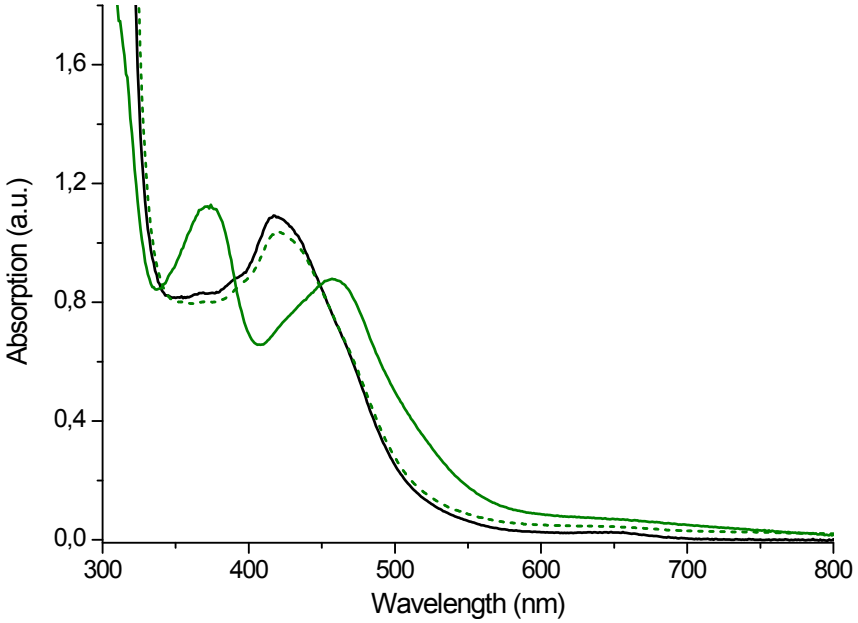

Figure S23. UV/Visible spectra of $[\mathbf{1}]^{2+}$ before photolysis (black plain line), after photolysis for 1h45 (green plain line) and after photolysis for 1h45 and exposition to air for 5 mn (green dashed line) at 193 µM in acetonitrile/propionitrile (1/2) (*EPR conditions*) using 0.25 M TEA as sacrificial electron donor. A 2 mm optical path cuvette was employed.